

# PCCP

Accepted Manuscript



This is an *Accepted Manuscript*, which has been through the Royal Society of Chemistry peer review process and has been accepted for publication.

*Accepted Manuscripts* are published online shortly after acceptance, before technical editing, formatting and proof reading. Using this free service, authors can make their results available to the community, in citable form, before we publish the edited article. We will replace this *Accepted Manuscript* with the edited and formatted *Advance Article* as soon as it is available.

You can find more information about *Accepted Manuscripts* in the [Information for Authors](#).

Please note that technical editing may introduce minor changes to the text and/or graphics, which may alter content. The journal's standard [Terms & Conditions](#) and the [Ethical guidelines](#) still apply. In no event shall the Royal Society of Chemistry be held responsible for any errors or omissions in this *Accepted Manuscript* or any consequences arising from the use of any information it contains.

# The new nanoparticles Pdots bind in their lipid modified surface *m*THPC and exhibit very high FRET efficiency between the core and the sensitizer

Sara Haupt<sup>a</sup>, Itay Lazar<sup>b</sup>, Hana Weitman<sup>a</sup>, Mathias O. Senge<sup>c</sup> and Benjamin Ehrenberg<sup>a</sup>

Cite this: DOI: 10.1039/x0xx00000x

Received 00th January 2012,  
Accepted 00th January 2012

DOI: 10.1039/x0xx00000x

www.rsc.org/

## Abstract

Pdots are a new type of nanoparticles which exhibit a strong promise for future applications in biophysics and cell biology. They are composed of organic chromophoric polymers, whose surface can be modified with different amphiphilic polymers, such as pegylated, lipids to make them very stable as colloids in water. We demonstrate in this manuscript that the lipid nano-coating around the Pdot can bind very efficiently amphiphilic molecules, such as photosensitizer e.g. meso-tetrahydroxyphenylchlorin (*m*THPC). As a result the sensitizer is brought to very close contact to the core of the Pdots, and resonance energy transfer from the core to the sensitizer is very efficient, in some cases close to 1. We show the spectroscopic properties of two types of Pdots, their size, which are in the 13-47 nm range, depending on the kind of polymer and the length of pegylated lipid chains that wrap it. We measured the efficiency of FRET by the decrease of donor intensity or its lifetime upon binding *m*THPC. We also show the relative yields of singlet oxygen that are obtained in the two pathways: by exciting the Pdots which transfer the energy to the attached sensitizer, or by exciting the sensitizer directly. This methodology could be used as an enhancer of using the photosensitizer by employing both pathways in parallel.

## INTRODUCTION

Nanoparticles have attracted great interest due to their promising potential for applications in biological sciences and other biomedical<sup>1,2</sup>, nanoparticles of gold, silicon, silica, metal oxides and several forms of carbon and the recently advanced semiconducting polymer dots (Pdots). Nanoparticles are used as drug-delivery vehicles, biosensors, imaging tools and markers, where their special chemical and optical properties are employed for analytical and diagnostic purposes<sup>3</sup>.

Quantum dots (QDs), especially, found the most wide-spread uses in scientific applications. They have narrow and size-dependent absorption and emission peaks with a considerable Stokes shift. Their absorption band is so wide that multiple excitation sources are not required for different QD types and sizes<sup>4,5</sup>. They have thus been extensively used as highly sensitive chemical and biological sensors and in live cell imaging<sup>6-12</sup>. Semiconducting polymer dots (Pdots), which we describe here, on the other hand, are nanoparticles that are obtained by mixing high molecular weight chromophoric polymers with various amphiphilic molecules such as phospholipids<sup>13-14</sup>. They share some properties with QDs, such as exhibiting a very strong absorption spectrum and strong brightness, a narrow emission bands and symmetric emissions with improved brightness and photostability<sup>15-21</sup>. They do not have a size-dependent absorption and emission spectra.

Photodynamic therapy (PDT)<sup>22-25</sup> is a relatively new selective method in cancer treatment. PDT is a promising approach to cancer treatment, in which a photosensitizer dye, upon exposure to light of the required wavelength, generates the excited level of molecular oxygen, singlet oxygen (<sup>1</sup>O<sub>2</sub>), as well as other radical species. <sup>1</sup>O<sub>2</sub> is highly cytotoxic, causing oxidative destruction of the cells in which it has been generated, which causes damage to the cell's membrane and internal organelles. Illumination also elicits the dye's fluorescence, which is used to mark the tumor's borders. Because of the preferential uptake of porphyrins by malignant tissue, the local illumination and the short life of the active species that are generated, no harmful effects are observed far from the tumor. PDT is being used for tumors of skin, lung, breast, bladder and others and has also been applied to eliminate viruses and bacteria.

It has been proposed to attach photosensitizers to nanoparticles and use them as a combined system to carry out PDT. The mode of the attachment spanned from covalent binding, on one hand, up to a "loose" electrostatic binding, on the other hand. Both methods were not pursued and expanded<sup>26,27</sup>. In this study, we propose to study a new approach to nanoparticles-sensitizer interaction by employing Pdots. The additional advantage of Pdots is that they are coated by an amphiphilic shell to make them water water-miscible, and this coating can also be used as a nano-environment into which the amphiphilic or hydrophilic photosensitizer can intercalate non-covalently, but with a high binding constant. If the Pdots' polymers, the donor, and the sensitizers, the acceptor, are chosen such that the donor's emission spectrum and the sensitizer's absorption spectrum exhibit a good overlap, a fluorescence radiation energy transition (FRET)<sup>28,29</sup> can occur. We therefore anticipate that since the absorption spectrum of Pdots' material is broad, a large fraction of the visible light will be absorbed by the Pdots, and it will be channelled into the sensitizer via a FRET mechanism. The crucial point here is that one can gain from the Pdots' absorption of light by absorbing wavelengths shorter than those absorbed by the sensitizer, because the Pdots' band is so broad so that their overall optical cross-section is high. If the FRET efficiency is high, the overall funnelled energy to the sensitizer might compensate for the FRET

research. Among the important nanostructures that have found use in biology and medicine one can list quantum dots (QDs

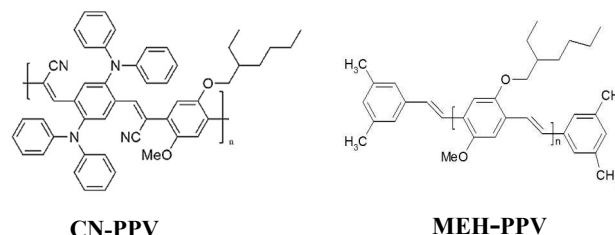
efficiency. These considerations have to be taken into account when using the Pdots-sensitizer composite structure for a more efficient mechanism of biological sensitization.

Our aim in this paper is to demonstrate the spectroscopic properties of two new types of Pdots, with broad absorption in the visible range, up to the near infrared. We demonstrate their spectroscopic properties and also their efficient FRET interaction with the well-established photosensitizer meso-tetrahydroxyphenylchlorin (*m*THPC).

## EXPERIMENTAL

## Chemicals

The polymers poly[2-methoxy-5(2-ethylhexyloxy)-1,4-phenylenevinylene] (ADS100RE, MEH-PPV; MW =>100,000), and polymer poly[2-methoxy-5(2-ethylhexyloxy)-1,4-(1-cyanovinylphenylene)-co-{2,5-bis(N,N'-diphenylamino)-1,4-phenylene}] (ADS100RE, CN-PPV-DPD; MW 15000-50000) were obtained from American Dye Source (Quebec, Canada). Their molecular structures can as be seen in Graph 1.



Graph 1: Chemical structures of polymers; MEH-PPV and CN-PPV

The following phospholipids were used for the amphiphilic shell: 1,2-dipalmitoyl-*sn*-glycero-3-phosphoethanolamine-*N*-[methoxy (polyethyleneglycol)-350] (PEG<sub>350</sub>-PE), which contains 7 PEG units and 1,2-dipalmitoyl-*sn*-glycero-3-phosphoethanolamine-*N*-[methoxy (polyethyleneglycol)-2000] (PEG<sub>2000</sub>-PE), containing 45 PEG units. They were purchased from Avanti Polar Lipids (Alabaster, AL, USA). In addition, we used natural egg-yolk lecithin, from Avanti Polar Lipids, in which the composition of fatty acids is as follows: 33% palmitic (C16:0), 31% oleic (C18:1), 13% stearic (C18:0), and 15% linoleic (C18:2). The remaining 8% is a mixture of several other fatty acids. meso-tetrahydroxyphenylchlorin (*m*THPC) was prepared by one of us (MS), as described by Bonnett *et al.*<sup>30</sup> 9, 10-Dimethylanthracene (DMA) was purchased from Sigma-Aldrich (St. Louis, MO). Tetrahydrofuran was purchased from Bio-Lab (Jerusalem, Israel) and dichloromethane was purchased from Carlo Erba Reagents (Rodano, Italy); both were of analytical grade.

## Preparation of Pdots

The Pdots have been synthesized by two main routes: the miniemulsion and the reprecipitation method. The miniemulsion method is using ultrasonication to form stable miniemulsions containing small droplets of the polymer solution. While the reprecipitation method is taking advantage of the conformational change brought about by introduction of the hydrophobic polymer into an aqueous solvent.

Particle synthesis using the miniemulsion method: 2 mg of the conjugated polymer MEH-PPV were placed in 15 mL of dichloromethane (DCM) and were stirred for 48 hours to maximize its solubilization. The solution was filtered using a 0.2  $\mu\text{m}$  membrane filter. Next, 4 or 7 mg of PEG<sub>350</sub>-PE, PEG<sub>2000</sub>-PE, and 5.22, 3.45 mg of lecithin were added, respectively, to maintain a constant PEGylated PE-to-lecithin ratio. The solution was mixed for 10 minutes and was then added to 20 mL of once-distilled water, under constant mixing. After sonication of the solution for 30 seconds by a Ti-probe sonicator (MSE Soniprep 150, Crawley, UK) it became homogeneous. The solution was paper-filtered immediately and centrifuged for 30 min at 2500 rpm. At this stage, the solution separated into two phases, an upper aqueous phase and a lower organic phase, which was discarded. To determine the Pdot's concentration in the aqueous suspension, we measured the amount of substance that was lost throughout the procedure of preparation at each step. The yield of the preparation of Pdots was 76% for PEG-PE<sub>350</sub> coating and 54%, for PEG<sub>2000</sub>-PE coating. The concentration of the Pdots' dye material in the final aqueous stock suspension was 1.52 and 1.09 mg/mL, respectively. The aqueous suspension remained stable for several weeks.

Particle synthesis procedure using reprecipitation method: applied to prepare coated nanoparticles composed of the polymer MEH-PPV utilized tetrahydrofuran (THF). The quantities of the material were identical to the previous preparation. The preparation process until the stage of sonication was identical to the preparation with DCM. The sonication of the solution was done for 30 seconds in an ultrasonication bath (Elmasonic s 30, 37 kHz, Singen, Germany). After sonication the solution was flushed with nitrogen to remove the THF and was centrifuged for 30 min. at 2500 rpm. The yield of the preparation was 42% for PEG-PE<sub>350</sub> coating and 47% for PEG<sub>2000</sub>-PE coating. The concentration of the Pdots' dye material in the final aqueous suspension was 1.15, 1.06 mg/mL, respectively.

Nanoparticles were also prepared with the polymer CN-PPV with THF. The procedure was identical to the preparation with the MEH-PPV polymer. The yield of the preparation was 94% for PEG<sub>350</sub>-PE coating and 93% for PEG<sub>2000</sub>-PE coating. The concentration of the Pdots' dye material in the final aqueous suspension was 1.89, 1.86 mg/mL, respectively.

#### Characterization of Pdots: Size and Surface

Dynamic light scattering (DLS). Analyses were performed with Cordouan Technology VASCO particle size analyzer (Nano Instruments Ltd, Pessac, France), with a laser wavelength of 658 nm. All data were obtained in a multi-acquisition mode, on 100 measurement runs with a time step of 50 s. In order to obtain good statistical information on size dispersion of the sample, the NanoQTM software of VASCO was operated in the multi-acquisition mode with each correlogram acquisition processed by the Padé-Laplace inversion algorithm<sup>31</sup>.

Atomic Force Microscopy (AFM). All scanning probe microscopy scans were performed using a MultiMode AFM with Nanoscope V electronics (Bruker AXS SAS, Santa Barbara, CA). The root-mean-square roughness (Rq) was calculated from  $2 \times 2 \mu\text{m}^2$  micrographs. All samples were scanned with a tapping mode, using a FESP silicon probe (force constant 1–5 N/m, Bruker). The fast scan direction was perpendicular to the cantilever's long axis, and the images were captured in the retrace direction with a scan rate of 1 Hz at pixel resolution of 512 samples/line. Before analysis of the images, first order "flatten" and "plane fit" functions were applied to each image. The roughness was determined by Nanoscope analysis software.

High Resolution Scanning Electron Microscopy (HR-SEM). The surface morphology of the Pdots was assessed by HR-SEM

(Magellan 400L, FEI) using an accelerating voltage of 5 kV with surface iridium coatings of approximately 30 nm thickness.

#### Spectroscopic Measurements

Absorption spectra were registered on a Shimadzu (Kyoto, Japan) UV-2501PC UV–visible spectrophotometer. Fluorescence excitation and emission spectra and fluorescence time-drive traces were measured on a Perkin-Elmer LS-50B digital fluorimeter (Norwalk, CT).

#### Singlet Oxygen Quantum Yield

We prepared aqueous suspensions of Pdots at concentration of 10  $\mu\text{g/mL}$  and 2  $\mu\text{M}$  9, 10-dimethylanthracene (DMA). DMA was used as a target for singlet oxygen, since it reacts selectively and efficiently with it to form the non-fluorescent 9, 10-endoperoxide (DMAO<sub>2</sub>). A diode-pumped solid state laser (Ningbo Lasever Inc., Ningbo, China) beam at 473 nm was chosen such that its radiation wavelength was in an absorption band of the Pdots. **In a similar** way we choose a diode-pump solid state laser beam at 650nm which is suitable for the absorption of *m*THPC. A power meter (Ophir Nova, Jerusalem, Israel) was used to determine the laser's power. A fluorescence time-drive experiment was run while irradiating the sample by the laser, and the decreasing intensity of DMA, due to its photo-oxidation, was monitored. The sample was stirred with a magnet during the time-drive run to ensure a proper homogeneous spread of light, DMA and the products of its decay throughout the cuvette.

#### Graphic and curve-fitting analyses

The rate of photon absorption by the sensitizer,  $k_{\text{pho}}$ , is given by Equation 1:

$$k_{\text{pho}} = \frac{0.98 \cdot P(1 - 10^{(-\text{abs} \cdot L)})}{E \cdot V} \quad (1)$$

Where P is the power of the laser in mW, abs is the optical density of the sample at the irradiated wavelength, L is the path length traversed by the laser beam through the sample, E is the Einstein units of light energy per second per watt of light at the irradiating wavelength and V is the volume of the sample in the cuvette in mL. The factor 0.98 corrects for the light reflected at the air/liquid interface.

The fluorescence intensity decay of DMA was fitted to an exponential Equation, by Origin (Microcal Software, Northampton, MA). As described in Equation 2:

$$I_{\text{DMA}} = A e^{-k_{\text{DMA}} t} \quad (2)$$

The quantum yields (QY) of singlet oxygen's production are proportional to the rate of DMA's photodestruction,  $k_{\text{DMA}}$ , normalized by light absorption,  $k_{\text{pho}}$  of Equation 1, as described in Equation 3:

$$QY_{\text{Pdot}/m\text{THPC}} \propto \left( \frac{k_{\text{DMA}}}{k_{\text{pho}}} \right)_{\text{Pdot}/m\text{THPC}} \quad (3)$$

#### Fluorescence quantum yields

To determine the fluorescence quantum efficiency of the Pdots, a comparison was performed with rhodamine 6G as a standard, whose quantum efficiency in ethanol is known to be 0.94<sup>32</sup>.

Quantum efficiencies of the Pdots were estimated using Equation 4:

$$Q_{PD} = \frac{OD_{ref}}{OD_{PD}} \cdot \frac{I_{PD}}{I_{ref}} \cdot \frac{n_{PD}^2}{n_{ref}^2} \cdot Q_{ref} \quad (4)$$

Where  $Q_{PD}$  and  $Q_{ref}$  are quantum efficiencies of the fluorescence of rhodamine 6G and Pdots,  $I_{PD}$  and  $I_{ref}$  are their integrated fluorescence intensities, respectively,  $OD_{PD}$  and  $OD_{ref}$  are their absorption coefficients,  $n_{PD}$  and  $n_{ref}$  are the refractive indexes of the materials in water and ethanol, respectively.

### Binding constants, $K_b$

The binding constant ( $K_b$ )<sup>33</sup> of *m*THPC to the Pdots was measured by monitoring the fluorescence intensity of *m*THPC, in aqueous solution, upon addition of increasing amounts of Pdots. The titration curve was used to monitor  $K_b$ . Following each added batch, overnight incubation period was found to be sufficient to achieve equilibrated binding.

### FRET Efficiency

We calculated the FRET efficiency from the various Pdots to *m*THPC bound to them, by two methods: measuring the change in fluorescence intensity of the donor, in stable condition, or by measuring the donor's fluorescence lifetime, under similar conditions. Both are shown in Equation 5.

$$E = 1 - \frac{I_{DA}}{I_D} = \frac{1}{1 + \left(\frac{r}{R_0}\right)^6} = 1 - \frac{\tau_{DA}}{\tau_D} \quad (5)$$

$I_{DA}$  and  $I_D$  are the emission intensity of the donor molecules in the presence and absence of the acceptor molecule (or the donor's fluorescence lifetime with or without the acceptor,  $\tau_{DA}$  and  $\tau_D$ ), respectively.  $r$  is the distance between the donor and acceptor pair and  $R_0$  is the Förster distance, the distance between the donor and acceptor at which the energy transfer is (on average) 50% efficient.  $R_0$  depends on  $J$ , representing the extent of overlap between the donor's fluorescence spectrum and the acceptor's absorption spectrum, respectively, Equation 7 below,  $\kappa^2$  - the orientation factor,  $n$  - the refractive index of the medium, and on  $Q_0$  - the fluorescence quantum yield of the donor in the absence of the acceptor, as described in Equation 6<sup>34</sup>.

$$R_0^6 = 8.79 \cdot 10^{-5} \cdot \kappa^2 \cdot n^{-4} \cdot Q_0 \cdot J \quad (6)$$

$$J = \int f_D(\lambda) \cdot \varepsilon_A(\lambda) \cdot \lambda^4 d\lambda \quad (7)$$

$f_D(\lambda)$  is the wavelength-dependent donor's normalized emission spectrum and  $\varepsilon_A(\lambda)$  is the extinction coefficient spectrum of the

### Time - Resolved Fluorescence Measurements

A home-built system at Bar Ilan University employs Time-Correlated Single Photon Counting. The excitation source has a femtosecond mode-locked Ti:Sapphire laser (Chameleon Ultra II, Coherent, Santa Clara, CA). The laser pulse width was 140 fs before doubling. A pulse selector (A.P.E, Berlin) was used to reduce the basic 80 MHz pulse rate to 4 MHz

The output frequency was multiplied by a flexible second- and third-harmonics generator (A.P.E., Berlin). The second harmonic was used for excitation at 480 nm. The emission was collected with a polarizer at a magic angle relative to the excitation polarizer at 590 nm. Measurements were taken at 25°C. The emission wavelength was selected by a double 1/8 m subtractive monochromator, with an emission slit width of 32 nm (DIGIKROM CM112), and directed to the surface of a PMT (Hamamatsu, R9880U-210) biased at -1100 V. A single-photon counting board (SPC 630, Becker & Hickel GmbH) fed via a preamplifier (HFAC-26DB 0.1UA) and triggered by a photodiode (PHD-400N) was used. Life Time Analysis was done by the Marquardt nonlinear least-squares Method<sup>35</sup>.

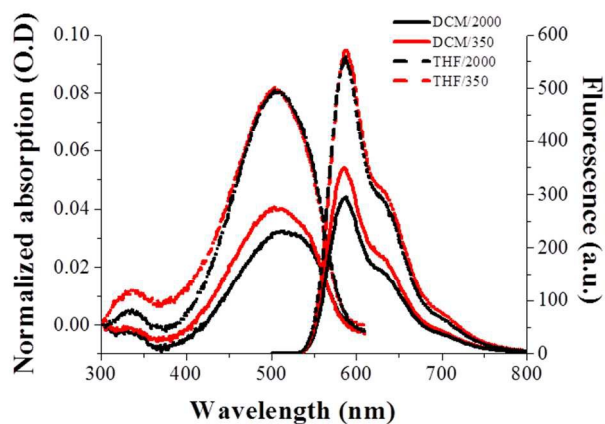
### RESULTS

In this paper, we explored the spectroscopic, energy-transfer and structural properties of the new nanoparticles, Pdots, as a tool in biophysical studies. Pdots have strong light absorption and we will show they also have a high efficiency of transferring energy to non-covalently attached molecules, such as sensitizers to generate singlet oxygen. This approach aims to use Pdots to increase the effectiveness of lipophilic molecules, such as sensitizers, that attach to the Pdots. The enhancement arises from the fact that the Pdots absorb light in a very broad spectral range and might transfer energy by FRET to the attached molecule, which absorbs light at a higher wavelength. Naturally, each excitation of the sensitizer via FRET will be somewhat less efficient than the direct excitation. But the polymer can utilize a much broader wavelengths' range, exhibiting a high integrated absorption cross-section. Thus, the FRET route may add a lot to the photosensitization process, because of the wide range of light wavelengths that could be used, even non-coherent white light.

### Spectroscopic properties of the MEH-PPV Pdots

We coated the Pdots that were composed of MEH-PPV with 60% lecithin and 40% PEG-PE, to make them water-dispersible. This coating stabilizes the particles in water and forms the amphiphilic nano-environment into which the amphiphilic sensitizer intercalates.

We show a comparison of the behaviour of Pdots that were produced by using the reprecipitation method (with THF solution) and the miniemulsion method (with DCM solution). In addition, we examined the influence of the two types of lipid and pegylated lipid coatings, which differ in the PEG-PE chain length (350 and 2000) with each of the different preparations. The absorption and fluorescence spectra of the Pdots composed of either of the two polymers, and with the two coatings are presented in Graph 2. The absorption peak of the Pdots is at 500 nm while the central fluorescence peak is at 590nm.



**Graph 2:** The absorption and fluorescence spectra of Pdts prepared with two types of polymers and two coating lengths: Full line – preparation with DCM solution; dotted line – preparation with THF solution. Black line – 2000 long coating; red line – 350 long coating.

The graph demonstrates that the spectra of the Pdts with the different coatings are identical; thus, the type of coating does not change the spectroscopic qualities of the polymer. In addition, the graph illustrates that spectra of Pdts obtained by both types of preparations (THF and DCM) are also identical. Therefore, the type of preparation does not affect the spectral qualities of the polymer either. In contrast, there is a difference in the fluorescence intensity of the two preparations: the Pdts prepared with the THF solution have higher fluorescence intensity than those prepared from the DCM solution. We assume that since THF is more polar than DCM, the contact area between the water phase and organic solvent during the preparation of the Pdts is different. These differences may affect the folding of the polymer within the globule. In addition, it is possible that preparing the Pdts in a sonication-bath as compared to a much powerful probe sonication influences the polymer in a different way, because of the stronger heat effect and cavitation with the probe sonication.

In addition, we examined the fluorescence quantum yields of the Pdts, by comparison to rhodamine G6, whose fluorescence quantum yield in ethanol is 0.95. The results were the following: the calculated fluorescence quantum yields of Pdts prepared in DCM was 0.045 and 0.04 in lipid with PEG-PE<sub>350</sub> and PEG-PE<sub>2000</sub> coatings, respectively. In contrast, when the Pdts were prepared in the THF solution, the fluorescence quantum yields obtained was 0.164 and 0.225 for the same lipids, respectively. Thus, the type of preparation affects the quantum yield of Pdts. This result supports the hypothesis that the polymer MEH-PPV is better dissolved in a THF solution than in DCM, which affects the production of the Pdts and the possibility that the difference in the preparation methods of the Pdts influences the polymer in a different way. In contrast, the length of the coating does not indicate a significant difference.

### The size of the particles

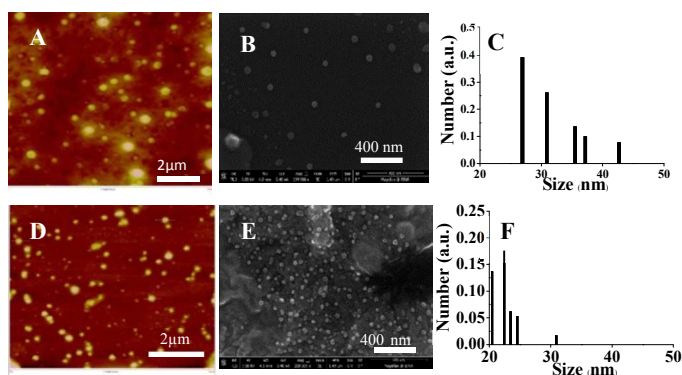
In order to characterize the size of the Pdts, we used AFM, which present nanometric sizes according to the different type of preparation and coating. We discovered that when the Pdts were prepared from the THF solution, the size was ~10 and ~20 nanometer with coatings of PEG<sub>350</sub>-PE chain lengths and PEG<sub>2000</sub>-PE chain lengths, respectively. In contrast, preparing the Pdts with DCM gave sizes of ~20 and ~40 nm for the same coatings, respectively. When we measured the surface of the Pdts by HR-SEM, we obtained sizes similar to those measured by the AFM and the ratio between the Pdts with the different coating lengths was

preserved. When we measured the diameter of the particles by means of a DLS, we obtained an identical ratio between the Pdts with the different coating lengths, but the mean size were larger than by AFM and HR-SEM. We attribute this to the inclusion of the hydrodynamic layer around the particle that moves with it to the moving particle, and not only the diameter of the core of the particles. The mean results obtained by the various measurements appear in Table 1.

	reprecipitation method		miniemulsion method	
	PEG <sub>350</sub> -PE in nm	PEG <sub>2000</sub> -PE in nm	PEG <sub>350</sub> -PE in nm	PEG <sub>2000</sub> -PE in nm
AFM	25	13	41	17
HR-SEM	26	14	42	18
DLS	31	23	48	27

**Table 1:** Mean size distribution of the Pdts in the different preparation methods and coating lengths, as measured by AFM, HR-SEM and DLS.

Graph 3 presents a qualitative comparison of the Pdts with different coating lengths prepared from the THF solution. Illustrations [A-C] are of Pdts coated by PEG<sub>2000</sub>-PE and illustrations [D-F] are of Pdts with coating of PEG<sub>350</sub>-PE.



**Graph 3:** The size of Pdts prepared from a THF solution. A and D are AFM pictures of the Pdts with coatings of PEG<sub>2000</sub>-PE and PEG<sub>350</sub>-PE, respectively. B and E are HR-SEM pictures of Pdts with PEG<sub>2000</sub>-PE and PEG<sub>350</sub>-PE, respectively. C and F show the results of the mean size of Pdts with coatings of PEG<sub>2000</sub>-PE and PEG<sub>350</sub>-PE lipids, respectively, as measured by DLS.

### Energy transfer between Pdts and *m*THPC – FRET efficiency

In this section we show the efficiency of energy transfer between the Pdts and the sensitizer which is attached to them. We linked the Pdts with the known photosensitizer, *m*THPC, which is commonly used in biological photosensitization and is known for its large efficiency of production of singlet oxygen<sup>26, 36</sup>. The central absorption peak of this photosensitizer is at 430nm and an additional peak is at 650 nm, while the fluorescence peak is at 653 nm. Therefore, the fluorescence peak of the Pdts overlaps nicely with the absorption band of *m*THPC and they are suitable to be used as a donor-acceptor pair and the efficiency of the energy transfer between them can be calculated.

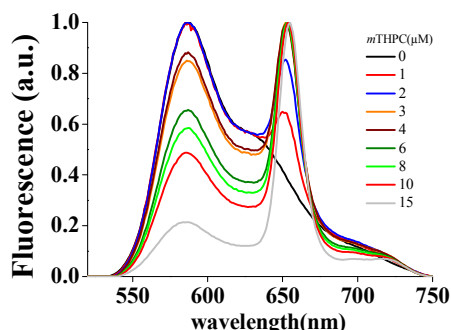
To get the most efficient energy transfer, we first measured the *m*THPC binding constant,  $K_b$ , to Pdts, by titrating the *m*THPC with the Pdts and tracing the fluorescence intensity. These results are shown in Table 2. The intuitive way to understand  $K_b$  is that at a Pdts concentration of  $1/K_b$ , half of the *m*THPC is bound.

Method K <sub>b</sub> of <i>m</i> THPC to Pdots composed of:	reprecipitation method	miniemulsion method
PEG <sub>350</sub> -PE	0.585 (μg/ml) <sup>-1</sup>	0.0876 (μg/ml) <sup>-1</sup>
PEG <sub>2000</sub> -PE	0.469 (μg/ml) <sup>-1</sup>	0.07 (μg/ml) <sup>-1</sup>

**Table 2:** The *m*THPC binding constant, K<sub>b</sub>, to the Pdots made various methods.

Table 2 demonstrate the binding constant of the *m*THPC to Pdots at extremely low concentration of Pdots. This low binding constant is expected considering the high hydrophobicity of the *m*THPC.

In order to see the effect of energy transfer between the Pdots and *m*THPC, we excited the Pdots at 485 nm, a wavelength at which *m*THPC has very low absorption and the absorption is mostly due to the Pdots. We have also found this wavelength to have the highest ratio of Pdots-to-*m*THPC absorption. The sample contained Pdots at a fixed concentration of 10 μg/mL when the reprecipitation method was used and 60 μg/mL when the miniemulsion method was used, accordingly with the K<sub>b</sub> ratio. We then added to the samples increasing concentration of *m*THPC (0-15 μg/mL). Graph 4 shows, as a comparative example, the energy transfer process between Pdots prepared from miniemulsion method with PEG<sub>350</sub>-PE coating and *m*THPC. Since the process of intercalation of *m*THPC to the coating of the Pdots is slow, and reaches equilibrium after up to a day, which is the time until we got stable fluorescence intensity at *m*THPC, we had to wait until the system Pdots-*m*THPC had equilibrated. Graph 4 demonstrates that the fluorescence intensity of the Pdots decreases as the concentration of *m*THPC in the solution increases and demonstrates FRET-driven emission.



**Graph 4:** Fluorescence of 10 μg/mL MEH-PPV-PEG<sub>350</sub>-PE Pdots with 0-15 μM *m*THPC (λ<sub>exc</sub> = 485 nm).

In order to assess, quantitatively, the results of the FRET process between the pair of Pdots and *m*THPC, we calculated the efficiency of the energy transfer between them. This efficiency is based on calculation of the relative area of the decreasing fluorescence curve as a result of adding *m*THPC to the solution. Table 3 presents the results of the energy transfer, calculated by Equation 5. The table demonstrates that the type of Pdots' preparation does not significantly affect the efficiency of the energy transfer, when Pdots with identical coating are compared. However, when the same types of Pdots with different coating lengths are compared, a clear trend is observed: longer coating induces more efficient FRET, until they coincide. We assume that due to the length of the PEGylated lipid coating, a more "dense" nanosized bundle of lipid and PEG chains is formed on the surface of the nanoparticle. This coating, which is

much longer for the PEG<sub>2000</sub>-PE than for PEG<sub>350</sub>-PE, affects the efficiency of FRET.

<i>m</i> THPC (μM)	miniemulsion method		reprecipitation method	
	PEG <sub>2000</sub> -PE	PEG <sub>350</sub> -PE	PEG <sub>2000</sub> -PE	PEG <sub>350</sub> -PE
0	0	0	0	0
1	0.27	0.25	0.27	0.25
2	0.31	0.30	0.34	0.32
3	0.39	0.32	0.42	0.34
4	0.49	0.37	0.56	0.41
6	0.58	0.39	0.62	0.53
8	0.61	0.48	0.71	0.58
10	0.67	0.59	0.72	0.68
15	0.81	0.79	0.85	0.80

**Table 3:** The mean efficiency of the energy transfer between the Pdots (10 μg/mL of reprecipitation method and 60 μg/mL of miniemulsion method) and increasing concentration of *m*THPC (0-15 μg/mL) and with lipid coatings of PEG<sub>2000</sub>-PE and PEG<sub>350</sub>-PE.

In addition to calculating the FRET, we calculated the Förster radius the distance at which the FRET efficiency is 50%. The results when the Pdots were prepared with THF were 39.9 Å and 42.8 Å for a PEG<sub>350</sub>-PE coating and the PEG<sub>2000</sub>-PE coating, respectively. In contrast, when the Pdots were prepared with DCM, the Förster radius was 33.0 Å and 32.3 Å for the two coatings, respectively. Overall, both preparations and with both PEG-lipid coatings generate Pdots that, when binding *m*THPC, exhibit very efficient FRET. The Förster radius increases when using Pdots prepared with THF, indicating a more efficient FRET. This result derives from the difference in the fluorescence quantum yields between the various solvents. In contrast, the length of the coating has no significant effect.

In this case we could not employ the measurement of the lifetime of the Pdots as a tool to evaluate the FRET efficiency, by Equation 5, because the decay rate of the Pdots was very fast and the instrument does not measure lifetimes less than 1 ns with good accuracy.

#### Singlet oxygen quantum yield

The production of singlet oxygen is the final aim and indication of success of the overall process of transduction steps of energy, by direct excitation of the sensitizer or via FRET from the Pdot donors, and can constitute a measure for the FRET process. The measurement of the singlet oxygen quantum yield was done by means of the singlet oxygen quencher 9,10-dimethylanthracene (DMA). DMA is known for its very efficient chemical reaction with singlet oxygen so it serves as a quantitative singlet oxygen trap. DMA is fluorescent, and when it reacts with singlet oxygen, it forms a non-fluorescent peroxide<sup>37</sup>. We followed the fluorescence intensity of DMA by exciting it at 360 nm, the probing wavelength, and the fluorescence intensity was measured at 430 nm, the major fluorescence peak of DMA. The decay of the DMA was examined in a solution with Pdots alone. This solution was illuminated with a laser diode at a wavelength of 473 nm. In addition, we examined two solutions that contained the pair *m*THPC-Pdots, with one solution illuminated with a laser diode at a wavelength of 473 nm in order to measure the singlet oxygen quantum yield due to the energy transfer between the Pdots and the *m*THPC. The second solution was illuminated with a laser diode at a wavelength of 650 nm, a wavelength that matches the absorption peak of the *m*THPC, in order

to measure the singlet oxygen quantum yield by direct excitation of *m*THPC.

The relative yield of singlet oxygen production and the error in the different types of preparations and lengths of coating were calculated by Equations 1-3, as shown in Table 4.

	miniemulsion method		reprecipitation method	
	PEG <sub>350</sub> -PE	PEG <sub>2000</sub> -PE	PEG <sub>350</sub> -PE	PEG <sub>2000</sub> -PE
$\frac{QY_{Pdots+mTHPC}}{QY_{Pdots}}$ EX:473 nm	3.26 ± 0.13	6.41 ± 0.27	3.61 ± 0.13	6.27 ± 0.23
$\frac{QY_{Pdots+mTHPC}(EX:473nm)}{QY_{Pdots+mTHPC}(EX:650nm)}$	0.33 ± 0.01	0.59 ± 0.026	0.61 ± 0.04	0.79 ± 0.05

**Table 4:** The relative singlet oxygen production by the pair *m*THPC-Pdots and Pdots alone, when excited at a wavelength of 473 nm (first line) as compared to the production of singlet oxygen by the pair *m*THPC-Pdots when excited at a wavelength of 473nm, and the pair *m*THPC-Pdots excited at a wavelength of 650 nm (second line), in the various lengths of the coating.

Table 4 demonstrates that when the Pdots-*m*THPC composite structures were excited at 473 nm, where the Pdots absorb, there was a stronger generation of singlet oxygen compared to Pdots alone (first line in the Table). This means, surprisingly, that the Pdots themselves generate singlet oxygen, though the generate of singlet oxygen is more productive when FRET occurs. In contrast, when the production of singlet oxygen is caused by the Pdots-*m*THPC composite structure, which is excited at a wavelength that matches the excitation of the Pdots, 473 nm, and the energy is transduced by FRET, it is less efficient than *m*THPC in the composite structure, which is excited directly (second line). The much higher concentration of Pdots than the *m*THPC caused almost complete binding and therefore the yield of <sup>1</sup>O<sub>2</sub> in Table 4 is independent of the extent of binding. The two values of relative <sup>1</sup>O<sub>2</sub> productions change between 0.61 and 0.79, which reflects on the FRET efficiencies, as all the numbers are normalized.

In addition, Pdots that were coated with longer PEG lipids had a stronger photosensitizing effect than with the short PEG lipid chains. This difference occurs in both types of preparations. We attribute this difference to the fact that the longer coating forms a denser and thicker nanosized bundle around the inner core of the polymeric chromophore. This form enables a thicker volume in which singlet oxygen can diffuse before escaping into the outside aqueous phase, and thus there is a better chance of meeting the target DMA molecule and reacting with it. We have observed this behaviour quite abundantly with photosensitizers in liposomal membranes.<sup>38</sup>

These results show a difference between the two types of preparation of Pdots. The solvent in which the polymer is dissolved before creating the Pdots affects its folding in the Pdot's core and also the fluorescent quantum efficiency of the polymer, as was discussed above. This effect, as shown, influences the other parameters, such as singlet oxygen production, FRET efficiency, etc.

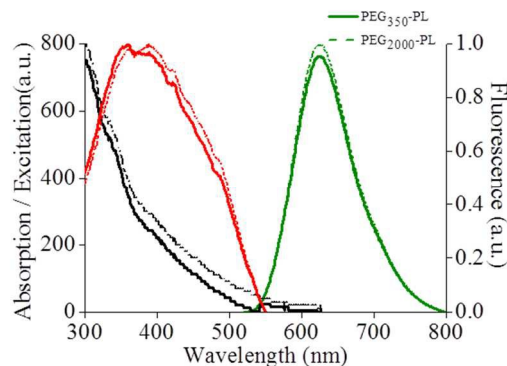
As we have mentioned above, the advantage of using the pair Pdots-*m*THPC in the dyad is the bigger light collection efficiency of the organic polymer in the Pdots, due to its broad and strong absorption spectrum. As a result, even if the FRET efficiency to the *m*THPC is slightly less than 1, the overall use of the wide light's bandwidth of the Pdots, in parallel to direct light absorption by the *m*THPC bring about a more efficient generation of singlet oxygen by the dyad than by the *m*THPC alone. At the concentrations that we used, namely 10 μg/ml MEH-PPV and 3 μM *m*THPC, at which the FRET efficiency was ~39% (Table 3), the Pdots constituted of 68% of the integrated absorption cross section in the whole region between 300 and 700nm

and *m*THPC contributed only 32%. This result proves the advantage in employing FRET in order to collect light energy by the Pdots.

### Spectroscopic properties of the CN-PPV Pdots

We produced Pdots from the polymer CN-PPV, shown in Graph 1. This polymer emits in the deeper red wavelength range, a region that currently is missing in this class of chromophores. The deeper red emission would also enable better overlap with longer-wavelength absorbing photosensitizers. This polymer was dissolved only in the THF solution, due to the results obtained with the polymer MEH-PPV, which were better in the reprecipitation method (THF solution), than miniemulsion method (DCM solution). The CN-PPV Pdots were coated with 60% lecithin and 40% PEG-PE for water stabilization. At this stage, we examined the influence of the same two types of coatings, which differ in the length of the PEG-PE chain.

The absorption, excitation and fluorescence spectra of the Pdots with the different coatings are presented in Graph 5. The absorption peaks of the Pdots are at 390 nm while the central fluorescence peak is at 624 nm. This is observed more clearly when the fluorescence excitation spectrum was taken, to eliminate the scattering. The graph demonstrates that the spectra of the Pdots with the two types of coatings are identical; thus, the type of coating does not change the spectroscopic qualities of the polymer.



**Graph 5:** Black line- Absorption, Red line- excitation and Green line- fluorescence spectra of CN-PPV-Pdots prepared with two coating lengths: Dotted line – PEG<sub>2000</sub>-PE; Full line – PEG<sub>350</sub>-PE.

We measured the fluorescence quantum yield of these Pdots by comparison to rhodamine G6. The results were that the quantum yield was not influenced by the length of the Pdots' coating chain and were 0.27 and 0.23 for the PEG<sub>350</sub>-PE and PEG<sub>2000</sub>-PE coating, respectively. Thus, the length of the coating lipid does not result in a significant difference, just as we received in the MEH-PPV Pdots.

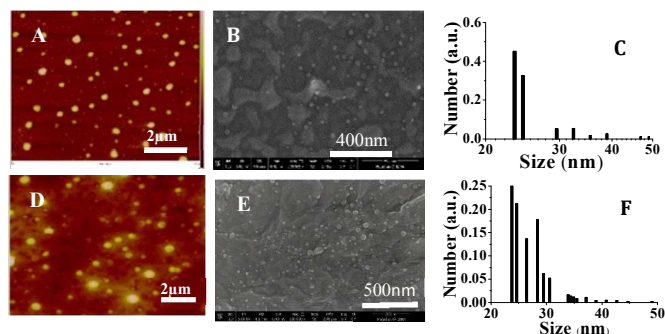
### The size of the particles

To characterize the surface of the Pdots, we used AFM, which present a small difference between the two types, of, Pdots coated with lipids with 350 and 2000 chain length, the results were ~15 nm and ~20 nm, respectively. The mean was taken by counting 100 particles. In order to characterize the morphology of the Pdots, we used HR-SEM and obtained practically identical sizes as was obtained by AFM. As with the MEH-PPV Pdots, the size measured by means of the DLS was larger, as a consequence of inclusion of the hydrodynamic layer. Table5 presents the mean size distribution of the Pdots with the various measuring instruments.

	PEG <sub>2000</sub> -PE in nm	PEG <sub>350</sub> -PE in nm
AFM	20	15
HR-SEM	20	16
DLS	27	22

**Table 5:** Mean size distribution of the Pdots with different lengths of the lipid coating as determined by different techniques.

Graph 6 presents a qualitative comparison of the Pdots with different coating lengths. The comparison was made by means of the AFM, HR-SEM and DLS instruments. Illustrations [A-C] are of Pdots coated by PEG<sub>350</sub>-PE and illustrations [D-F] are of Pdots with coating of PEG<sub>2000</sub>-PE.



**Graph 6:** The sizes of the Pdots. A and D are AFM pictures of the Pdots with coatings of PEG<sub>350</sub>-PE and PEG<sub>2000</sub>-PE, respectively. B and E are HR-SEM pictures of Pdots with PEG<sub>350</sub>-PE and PEG<sub>2000</sub>-PE, respectively. C and F show the results of the mean size of Pdots with coatings of PEG<sub>350</sub>-PE and PEG<sub>2000</sub>-PE lipids, respectively, as measured by DLS.

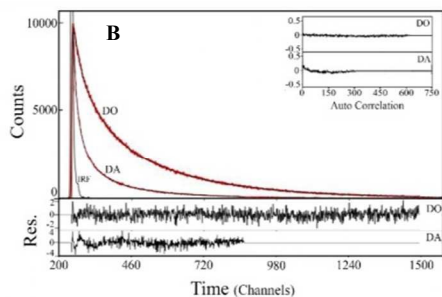
### Energy transfer between Pdots and *m*THPC – FRET efficiency

As with the polymer MEH-PPV, we linked the Pdots composed of CN-PPV to the *m*THPC. To get the most efficient energy transfer, we first measured the *m*THPC binding constants,  $K_b$ , to Pdots. The  $K_b$  of *m*THPC to Pdots composed of PEG<sub>2000</sub>-PE was  $0.661(\mu\text{g/ml})^{-1}$  and of PEG<sub>350</sub>-PE was  $0.399(\mu\text{g/ml})^{-1}$ . Since the polymer CN-PPV has measurable intrinsic fluorescence, we could measure its efficiency as a donor to *m*THPC. Graph 7 demonstrates the lifetime of the Pdots alone and the Pdots in the presence of *m*THPC. Where the DO line is the experiment with the donor-only and the DA curve is the experiment with the donor-acceptor. The analysis of fluorescence time-resolved FRET experiments is based on curve fitting methods. We obtained the average fluorescence lifetime of Pdots with increasing concentrations of *m*THPC. The average lifetime of the samples was determined from multiexponential analysis of the emission decay as described in Equation 8:

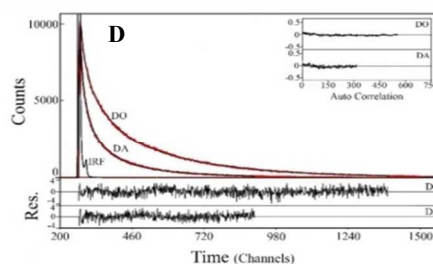
$$\langle \tau \rangle = \sum_i a_i \tau_i \quad (8)$$

Where  $\tau_i$  and  $a_i$  are lifetime and the relative amplitude of the  $i^{\text{th}}$  decay component respectively. The quality of the fitted curves to the experimental data is judged by the minimization of the  $\chi^2$  values. The strong decay rate of DA curve shown in Graph 7 is due to FRET effect.

A CN-PPV (PEG <sub>350</sub> -PE)					
<i>m</i> THPC (μM)	$\tau_1$ (a <sub>1</sub> )	$\tau_2$ (a <sub>2</sub> )	$\tau_3$ (a <sub>3</sub> )	$\langle \tau \rangle$ (ns)	$\chi^2$
0	14.92 (0.23)	4.70 (0.22)	0.73 (0.22)	6.87	1.1
1	12.93 (0.18)	3.51 (0.24)	0.56 (0.29)	4.73	1.11
2	12.71 (0.16)	3.59 (0.24)	0.57 (0.32)	4.27	1.25
3	12.29 (0.15)	3.16 (0.24)	0.51 (0.34)	3.79	1.16
4	11.46 (0.12)	2.07 (0.23)	0.41 (0.44)	2.75	1.31
5	9.83 (0.08)	2.09 (0.23)	0.33 (0.56)	1.7	1.29
6	9.31 (0.09)	1.87 (0.24)	0.29 (0.61)	1.52	1.37
7	8.99 (0.07)	1.68 (0.21)	0.25 (0.70)	1.18	1.42



B CN-PPV (PEG <sub>2000</sub> -PE)					
<i>m</i> THPC (μM)	$\tau_1$ (a <sub>1</sub> )	$\tau_2$ (a <sub>2</sub> )	$\tau_3$ (a <sub>3</sub> )	$\langle \tau \rangle$ (ns)	$\chi^2$
0	14.3 (0.21)	3.99 (0.21)	0.58 (0.31)	5.49	1.09
2	12.65 (0.17)	3.58 (0.21)	0.50 (0.36)	4.18	1.05
3	11.8 (0.14)	3.07 (0.20)	0.44 (0.43)	3.21	1.12
5	9.88 (0.09)	2.65 (0.21)	0.43 (0.43)	2.27	1.23
6	9.38 (0.10)	2.56 (0.23)	0.39 (0.51)	2.1	1.28



**Graph 7:** Fluorescence decay parameters for CNPPV Pdots with increasing concentrations of *m*THPC. The excitation was measured at 480 nm, where the Pdot's intrinsic chromophore absorbs almost exclusively and the emission is measured at 600 nm.  $\langle \tau \rangle$  is the average life-time of the Pdot. A and C demonstrate the mean lifetime of the donor, with coating of PEG350-PE and PEG2000-PE, respectively and the result of a  $\chi^2$  test. B and D demonstrate the fluorescence decay curves of the Pdots. The residuals (bottom) and the corresponding autocorrelation functions (upper right) served as indicators of the quality of the fit of the experimental data to a multiexponential function

Another measurement that points to the FRET efficiency is the decreasing fluorescence intensity of the Pdots. In order to quantitatively evaluate the FRET process between the pair Pdots and *m*THPC, we excited the Pdots at a wavelength of 485 nm. The sample contained Pdots, which served as a donor, at a fixed concentration of 10  $\mu\text{g/mL}$  to which we added increasing concentrations of *m*THPC, which served as the acceptor (0-15  $\mu\text{g/mL}$ ). In this case as well, the linking of *m*THPC to the coating of the Pdots needs long equilibration, up to a day. Table 6 presents the mean results of the energy transfer efficiency between the Pdots and *m*THPC: by measuring the donor's decreasing lifetime or by its decreasing fluorescence intensity (see Eq. 5). The table demonstrates that the type of coating affects the efficiency of the transfer and that the efficiency of the energy transfer in a coating of 2000 length is better. This supports the postulation that we have raised earlier that the coating with longer lipids "helps" bringing the *m*THPC molecule closer to the polymer. It can also be seen that because of a better overlap between the donor's emission, which occurs at longer wavelengths, and the acceptor's absorption spectra, FRET efficiency in this case reaches almost unity.

<i>m</i> THPC ( $\mu\text{M}$ )	PEG <sub>2000</sub> -PE		PEG <sub>350</sub> -PE	
	By donor's fluorescence intensity	By donor's fluorescence lifetime	By donor's fluorescence intensity	By donor's fluorescence lifetime
0	0	0	0	0
1	0.19	0.31	0.12	0.2
2	0.3	0.37	0.19	0.23
3	0.38	0.44	0.26	0.41
4	0.45	0.59	0.42	0.5
6	0.67	0.77	0.66	0.78
8	0.82	0.9	0.76	-
10	0.91	-	0.9	-
15	0.98	-	0.97	-

**Table 6:** The efficiency of the energy transfer between the Pdots with different coating lengths at a fixed concentration of Pdots (10  $\mu\text{g}/\text{mL}$ ) with increasing concentrations of *m*THPC (0-15  $\mu\text{g}/\text{mL}$ ) determined either by measuring the donor's fluorescence intensity or the by fluorescence lifetime. The data are averages of results obtained from 3 independent experiments.

We calculated the Förster radius (using Eq. 6) and found it to be 46.7 Å and 44.4 Å for PEG350-PE and PEG2000-PE coatings, respectively.

### Singlet oxygen quantum yield

We measured the production of singlet oxygen, the important parameter when Pdots are considered for photosensitization by a FRET mechanism.

At this stage too, the decay of the singlet oxygen target, DMA, was examined under several conditions: a sample containing Pdots alone, and illuminated by a laser diode at a wavelength of 473 nm; a sample containing the pair *m*THPC-Pdots, and singlet oxygen was generated via FRET after illuminating the Pdots solely; and one in which singlet oxygen was produced by direct illumination of *m*THPC. The relative yield of singlet oxygen production and the error in the different types of preparations and length of coating were calculated by Equations 1-3, as shown in Table 7.

	PEG <sub>350</sub> -PE in nm	PEG <sub>2000</sub> -PE in nm
$\text{QY}_{\text{Pdots}+m\text{THPC}}/\text{QY}_{\text{Pdots}}$ (EX:473 nm)	$2.38 \pm 0.08$	$3.07 \pm 0.1$
$\text{QY}_{\text{Pdots}+m\text{THPC}}(\text{EX:473nm}) /$ $\text{QY}_{\text{Pdots}+m\text{THPC}}(\text{EX:650nm})$	$0.92 \pm 0.05$	$0.99 \pm 0.05$

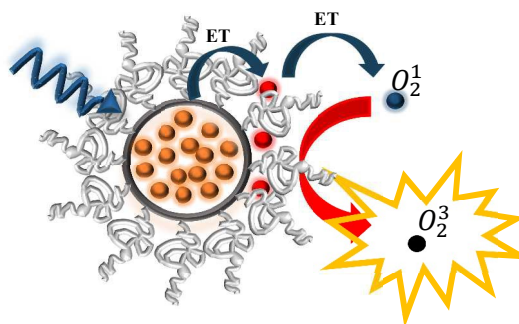
**Table 7:** The relative singlet oxygen production by the pair *m*THPC-Pdots and Pdots alone when excited at a wavelength of 473 nm (first line) as compared to the production of singlet oxygen by the pair *m*THPC-Pdots when excited at a wavelength of 473 nm, and the pair *m*THPC-Pdots excited at a wavelength of 650 nm (second line) for different coating lengths.

The first line of Table 7 demonstrates that the production of singlet oxygen by illumination of *m*THPC is 2-3 more efficient than by illuminating CN-PPV Pdots with the coatings PEG<sub>350</sub>-PE and PEG<sub>2000</sub>-PE, and relying on FRET to transduce the energy to *m*THPC, respectively. Still, these CN-PPV Pdots turns out to have some efficiency if producing singlet oxygen.

However, more importantly, when we compare the efficiency singlet oxygen generation by illuminating the Pdots followed by FRET to *m*THPC, relative to direct illumination of *m*THPC, the two yields are practically identical. See second line in the Table, in which absorbance and laser powers are all normalized. This proves that the

efficiency of the resonance energy transfer step is extremely high, almost one, and both pathways, by FRET or direct excitation of the sensitizer, are equally efficient.

It should be taken, however, into consideration that the indirect way leading to the production of singlet oxygen via FRET from the Pdots might practically be more important than by direct excitation of the photosensitizer. The reason for this is that the cross-section for absorption of light by the photosensitizer is small, because it is limited to a small region of spectral of light, where the sensitizer absorbs, in a small range of long wavelengths. However, the chromophore that constitutes the polymeric semiconductor has a very broad absorption spectrum, spreading over more than 150 nm. Therefore, the integrated cross-section for its absorption of light within that range is much higher. This is the reason for the high brightness of the Pdots and therefore its absorbance, as well as FRET to the sensitizer bound to it, is high.



### CONCLUSIONS

Pdots are known as nanoparticles composed of partially-conductive polymers. By mixing them with PEGylated phospholipids they can become water miscible and form stable colloids. After their preparation, the Pdots are stable for months and present very good absorption and fluorescence. In this article, we present two types of Pdots, prepared from different polymers: MEH-PPV and CN-PPV. We coated them with a mixture of lipids which endow them with this miscibility, but it also generates this lipid layer, into which amphiphilic molecules can intercalate. In this paper we demonstrate that the photosensitizer *m*THPC binds very efficiently to this lipid coating of the Pdots. The good binding and overlap between the emission spectrum of the Pdots and the absorption spectrum of the *m*THPC increase the efficient energy transition from the Pdots to the photosensitizer. We demonstrated that as a result of the energy transfer, *m*THPC serves as a sensitizer which is excited directly, and both indirectly, by FRET from the Pdots.

We also showed that there are detailed differences between the modes of the preparation of the Pdots. They express themselves in the fluorescence intensity, in the binding constant and in the size of the Pdots. Using **the reprecipitation** method yielded better results in these respects. This indicates that the initial solvent in which the polymer is prepared does influence the formation of the Pdots and their characterization, and may even be trapped in the organic polymer's core. The ability to find the solvent in which the polymer will "feel" best is the key to the efficiency of creating the Pdots.

A comparison between the Pdots prepared from the different polymers revealed differences in size and generation of singlet oxygen. The generation of singlet oxygen by the Pdots prepared from CN-PPV was greater than the generation of singlet oxygen by the Pdots prepared from MEH-PPV. In addition, singlet oxygen generated by the transfer of energy between the Pdots and the photosensitizer was practically identical to the singlet oxygen created by the photosensitizer itself. This confirms the usage of the composite structures (Pdots- *m*THPC) efficiency, when on the one

hand we have the wide spectrum absorption of the Pdots and on the other, the maximal efficiency of the generation of singlet oxygen. We also showed the effect of the length of the lipid chains that were used to wrap the organic core. The best results were obtained by the PEG2000-PE coating. The difference in size can be explained by the spatial arrangement of the coating. The PEGylated phospholipid which composes the coating is arranged itself in the form of a corm, so that the longer the coating, the larger the corm and the larger the Pdots. In contrast, when the coating is smaller, the corm created is smaller so that the volume obtained is smaller. The differences in the efficiency of energy transfer and generation of singlet oxygen can be explained by the fact that the entanglement created by the length of the coating "helps" the photosensitizer molecule, *m*THPC, to get closer to the core of the polymer. This process causes a more efficient FRET and a greater generation of singlet oxygen. This article demonstrates that it would be worthwhile to examine the use of Pdots in the field of biology. Future studies could examine whether the Pdots can improve the photodynamic treatment by serving as antennas for a wide range of wave lengths and not only in the red absorption range that exists today.

## Notes and references

<sup>a</sup> Department of Physics and Institute of Nanotechnology and Advanced Materials, Bar Ilan UnivDepartment of Physics and the Institute of Nanotechnology and Advanced Materials, Bar Ilan University, Ramat Gan, Israel, 52900; ehren@mail.biu.ac.il

<sup>b</sup> The Mina and Everard Goodman Faculty of Life Sciences, Bar Ilan University, Ramat Gan, Israel, 52900

<sup>c</sup> School of Chemistry, Trinity College Dublin, Dublin 2, Ireland.

- J. K. Jaiswal and S. M. Simon, Potentials and Pitfalls of Fluorescent Quantum Dots for Biological Imaging, *Trends Cell Biol.*, 2004, **14**, 497–504.
- M. De, P. S. Ghosh and V. M. Rotello, Applications of Nanoparticles in Biology, *Adv. Mater.*, 2008, **20**, 4225–4241.
- S. Bhattacharyya, S. Prashanthi, P. R. Bangal and A. Patra, Photophysics and Dynamics of Dye-Doped Conjugated Polymer Nanoparticles by Time-Resolved and Fluorescence Correlation Spectroscopy, *J. Phys. Chem. C.*, 2013, **117**, 26750–26759.
- A. P. Alivisatos, Perspectives on the Physical Chemistry of Semiconductor Nanocrystals, *J. Phys. Chem.*, 1996, **100**, 13226–13239.
- B. O. Dabbousi, J. Rodriguez-Viejo, F. V. Mikulec, J. R. Heine, H. Mattoussi, R. Ober, K. F. Jensen and M. G. Bawendi, (CdSe)ZnS Core-Shell Quantum Dots: Synthesis and Characterization of a Size Series of Highly Luminescent Nanocrystallites, *J. Phys. Chem. B.*, 1997, **101**, 9463–9475.
- W. C. W. Chan and S. Nie, Quantum Dot Bioconjugates for Ultrasensitive Nonisotopic Detection, *Scienc*, 1998, **281**, 2016–2018.
- J. K. Jaiswal, H. Mattoussi, J. M. Mauro and S. M. Simon, Long-term multiple color imaging of live cells using quantum dot bioconjugates, *Nature Biotechn.*, 2002, **21**, 47–51.
- X. Gao, Y. Cui, R. M. Levenson, L. W. K Chung and S. Nie, In vivo cancer targeting and imaging with semiconductor quantum dots, *Nature Biotechn.*, 2004, **22**, 969–976.
- X. Michalet, F. F. Pinaud, L. A. Bentolila, J. M. Tsay, S. Doose, J. J. Li, G. Sundaresan, A. M. Wu, S. S. Gambhir and S. Weiss, Quantum Dots for Live Cells, in Vivo Imaging, and Diagnostics, *Nature Mater.*, 2005, **4**, 826–831.
- A. Fu, W. Gu, C. Larabell and A. P Alivisatos, Semiconductor nanocrystals for biological imaging, *Curr. Opin. Neurobiol.*, 2005, **15**, 568–575.
- X. Michalet, F. F. Pinaud, L. A. Bentolila, J. M. Tsay, S. Doose, J. J. Li, G. Sundaresan, A. M. Wu, S. S. Gambhir and S. Weiss, Quantum Dots for Live Cells, in Vivo Imaging, and Diagnostics, *Science*, 2005, **307**, 538–544.
- M. Bruchez Jr, M. Moronne, P. Gin, S. Weiss, A. P. Alivisatos; Semiconductor Nanocrystals as Fluorescent Biological Labels, *Science*, 1998, **281**, 2013–2016.
- P. Howes, M. Green, J. Levitt, K. Suhling and M. Hughes, Phospholipid encapsulated semiconducting polymer nanoparticles: their use in cell imaging and protein attachment, *J. Am. Chem. Soc.*, 2010, **132**, 3989–3996.
- C. Szymanski, C. F. Wu, J. Hooper, M. A. Salazar, A. Perdomo, A. Dukes and J. McNeill, Single molecule nanoparticles of the conjugated polymer MEH-PPV, preparation and characterization by near-field scanning optical microscopy, *J. Phys. Chem. B.*, 2005, **109**, 8543–8546.
- I. L. Medintz, H. T. Uyeda, E. R. Goldman and H. Mattoussi; Quantum dot bioconjugates for imaging, labelling and sensing, *Nature Mater.*, 2005, **4**, 435–446.
- C. Wu, H. Peng, Y. Jiang and J. McNeill, Energy Transfer Mediated Fluorescence from Blended Conjugated Polymer Nanoparticles, *J. Phys. Chem. B.*, 2006, **110**, 14148–14154.
- C. Wu, C. Szymanski, Z. Cain and J. McNeill, Conjugated Polymer Dots for Multiphoton Fluorescence Imaging, *J. Am. Chem. Soc.*, 2007, **129**, 12904–12905.
- C. Wu, B. Bull, C. Szymanski, K. Christensen and J. McNeill, Multicolor Conjugated Polymer Dots for Biological Fluorescence Imaging, *ACS Nano*, 2008, **2**, 2415–2423.
- C. Wu and J. McNeill, Swelling-Controlled Polymer Phase and Fluorescence Properties of Polyfluorene Nanoparticles, *Langmuir*, 2008, **24**, 5855–5861.
- B. Vasudevanpillai, I. Tamitake, A. Abdulaziz, S. Athiyannathil and I. Mitsuru, Semiconductor quantum dots and metal nanoparticles: syntheses, optical properties, and biological applications, *Anal. Bioanal. Chem.*, 2008, **391**, 2469–2495.

21. K. Y. Pu, K. Li, J. B. Shi and B. Liu, Fluorescent Single-Molecular Core-Shell Nanospheres of Hyperbranched Conjugated Polyelectrolyte for Live-Cell Imaging, *Chem. Mater.*, 2009, **21**, 3816–3822.
22. T. J. Dougherty, Photosensitizers: therapy and detection of malignant tumors, *Photochem. Photobiol.*, 1987, **45**, 879–889.
22. B. W. Henderson and T. J. Dougherty, How does photodynamic therapy work?, *Photochem. Photobiol.*, 1992, **55**, 145–157.
24. S. Verma, G. M. Watt, Z. Mal and T. Hasan, Strategies for enhanced photodynamic therapy effects, *Photochem. Photobiol.*, 2007, **83**, 996–1005.
25. Z. Jiang, B. Dong, B. Chen, J. Wang, L. Xu, S. Zhang and H. Song, Multifunctional Au@mSiO<sub>2</sub>/Rhodamine B Isothiocyanate Nanocomposites: Cell Imaging, Photocontrolled Drug Release, and Photothermal Therapy for Cancer Cells, *Small*, 2013, **9**, 604–612.
26. J. M. Tsay, M. Trzoss, L. X. Shi, X. X. Kong, M. Selke, M. E. Jung and S. Weiss, Singlet oxygen production by peptide-coated quantum dot-photosensitizer conjugates, *J. Am. Chem. Soc.*, 2007, **129**, 6865–6871.
27. S. Moeno and T. Nyokong, Opposing responses elicited by positively charged phthalocyanines in the of CdTe quantum dots, *J. Photochem. Photobiol. A Chem.*, 2009, **201**, 228–236.
28. S. Bhattacharyya, B. Paramanik and A. Patra, Energy Transfer and Confined Motion of Dyes Trapped in Semiconducting Conjugated Polymer Nanoparticles, *J. Phys. Chem. C*, 2011, **115**, 20832–20839.
29. S. Bhattacharyya, M. K. Barman, A. Baidya and Amitava Patra, Singlet Oxygen Generation from Polymer Nanoparticles-Photosensitizer Conjugates Using FRET Cascade, *J. Phys. Chem. C*, 2014, **118**, 9733–9740.
30. R. Bonnett, R. D. White, U. J. Winfield and M. C. Berenbaum, Hydroporphyrins of the meso-tetra (hydroxyphenyl) porphyrin series as tumor photosensitizers, *Biochem. J.*, 1989, **261**, 277–280.
31. Z. Bajzer, A. C. Myers, S. S. Sedarous, and F. G. Prendergast, Padé-Laplace method for analysis of fluorescence intensity decay, *Biophys. J.*, 1989, **56**, 79–93.
32. M. Fischer and J. Georges, Fluorescence quantum yield of rhodamine 6G in ethanol as a function of concentration using thermal lens spectrometry, *Chem. Phys. Lett.*, 1996, **260**, 115–118.
33. B. Ehrenberg, Assessment of the partitioning of probes to membranes by spectroscopic titration, *J. Photochem. Photobiol. B. Biol.*, 1992, **14**, 383–386.
34. J. R. Lakowicz, Principle of Fluorescence Spectroscopy, Springer, New York, 2006.
35. J. M. Beechem and E. Haas, Simultaneous determination of intramolecular distance distributions and conformational dynamics by global analysis of energy transfer measurements, *Biophys. J.*, 1989, **55**, 1225–1236.
36. M. O. Senge and J. C. Brandt, Temoporfin (Foscan®), 5, 10, 15, 20-Tetra (m-hydroxyphenyl) chlorin)-A Second-generation Photosensitizer, *Photochem. Photobiol.*, 2011, **87**, 1240–1296.
37. F. Wilkinson, W.P. Helman and A.B. Ross, Rate Constants For the Decay and Reactions of the Lowest Electronically Excited Singlet State of Molecular Oxygen in Solution. An Expanded and Revised Compilation, *J. Phys. Chem. Ref. Data.*, 1995, **24**, 663–1021.
38. I. Bronshtein, M. Afri, H. Weitman, A. Frimer, K. M. Smith and B. Ehrenberg, Porphyrin Depth in Lipid Bilayers as Determined by Iodide and Parallax Fluorescence Quenching Methods and Its Effect on Photosensitizing Efficiency, *Biophys. J.*, 2004, **87**, 1155–1164.